Chapter: 3

Design and Development of L_nC_{2n-2} Network Based Multi-Output Hybrid Converter

3.1. Introduction

As discussed earlier, the demand for DC loads is increasing rapidly, creating a growing need for power systems that can efficiently supply both existing AC loads and the rising number of DC loads. Traditionally, this requires the use of two separate converters: one for AC loads and another for DC loads. However, this approach results in a cost-inefficient system, as it involves a higher number of switches and components, increasing both complexity and expense.

To address this issue, Multi-Output Hybrid Converters (MOHCs) have emerged as a promising solution. These converters are designed to supply both AC and DC loads simultaneously from a single input source, significantly reducing the number of components and switches required. This makes MOHCs more cost-effective and compact compared to the conventional dual-converter approach.

Despite their advantages, MOHCs face certain challenges. Since the same set of switches is used to regulate both AC and DC outputs, there is an inherent trade-off between the voltage gains of the two outputs. Specifically, the relationship between the duty ratio (d) and the AC voltage gain (m_i) imposes a constraint, expressed as $d + m_i \leq 1$. This makes it difficult to achieve standard voltage ratings for both outputs — such as 110V AC alongside 230V or 240V DC — simultaneously.

In this chapter, a novel MOHC design is proposed to overcome this limitation. The proposed converter not only supplies both AC and DC loads from a single input source but also ensures that the output voltages meet standard ratings without compromising

performance. This approach enhances the practicality and efficiency of hybrid power systems for modern energy demands.

3.2. Topology Development

In the proposed design, an inverter is replaced with the single switch of traditional DC-DC converters, resulting in a multi-output hybrid converter powered by a single input, as illustrated in Fig. 3.1. The core of this converter is an L_nC_{2n-2} network, which efficiently boosts the low input voltage from a photovoltaic (PV) source to align with the existing supply voltage rating.

A key advantage of this network is that it is expandable, and it can be expanded up to '*n*' stages. At each stage, a new 'K^{th}' cell is introduced, and each of these cells consists of one inductor, two capacitors, and one diode. This staged expansion enables flexible voltage gain, which is determined by the formula 1/(1-*nd*), where '*n*' represents the number of stages and 'd' is the duty ratio of the converter.

One of the distinctive features of this design is the simultaneous AC and DC operation achieved using the same set of switches. This introduces an interplay between the duty ratio (d), which governs the DC voltage gain, and the modulation index (m_i), responsible for the AC voltage output. To maintain proper operation, the sum of these two parameters must always remain below 1, i.e., $d + m_i \leq 1$.

As more stages (n) are added to the L_nC_{2n-2} network, the voltage gain increases even at lower duty ratios. This characteristic allows the system to achieve higher voltage output

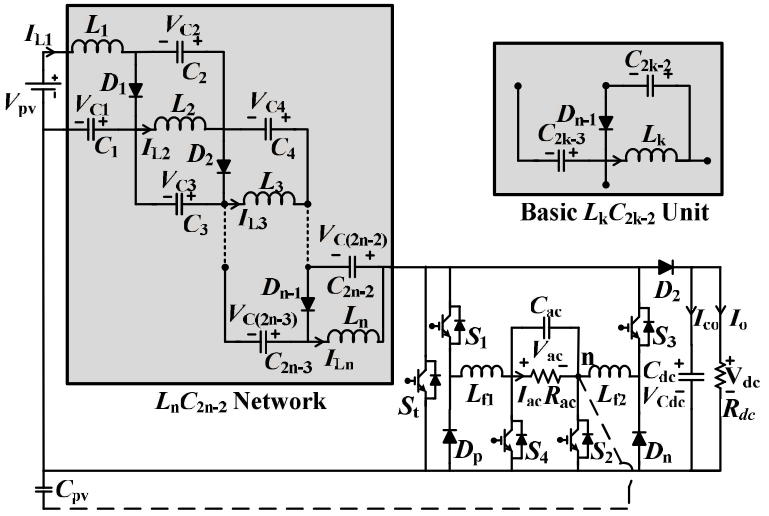

Fig.3.1 Proposed L_nC_{2n-2} network-based multi-output Hybrid converter.

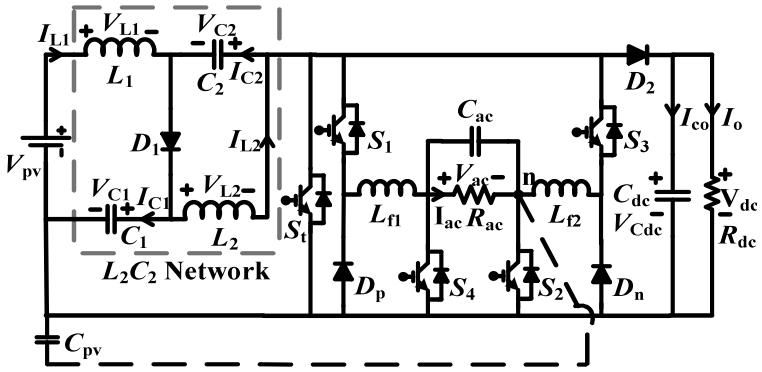

Fig. 3.2. Proposed L_2C_2-network-based multi-output Hybrid converter.

while maintaining a wider operating range for the modulation index (m_i). This feature enhances the converter's flexibility in various operating conditions.

For the validation of this proposed concept, a two-stage network (n = 2) was chosen, resulting in an L_2C_2-based multi-output hybrid converter (MOHC) as illustrated in Fig. 3.2. The operating modes and performance of this specific configuration are discussed in detail in the following section.

3.3. Proposed Circuit Operations and Switching

The proposed converter for n=2, i.e., L_2C_2 network-based multi-output Hybrid converter (L_2C_2-HC) comprises of L_2C_2 impedance network to boost the input voltage, and with the help of five switches (S_1, S_2, S_3, S_4, and S_t), three diodes (D_p, and D_n), two filter inductor (L_{f1}, and L_{f2}), one AC capacitive filter (C_{ac}) and one DC capacitive ripple filter (C_{dc}) a topology is formulated which is capable of supplying both DC and AC loads. The circuit operation and switching of the proposed L_2C_2-HC is discussed in the subsequent section.

3.3.1. Operating Modes

The operating modes of the L_2C_2-HC are categorized into three types, i.e., shoot-through, power, and zero modes of operation, for both V_{ac}>0 and V_{ac}<0, which are discussed below.

- **Shoot-through state:** This state of operation in the L_2C_2-HC converter plays a crucial role in its overall working. During this phase, the S_t switch remains continuously ON for both positive and negative cycles of the AC voltage ($V_{ac} > 0$ and $V_{ac} < 0$).

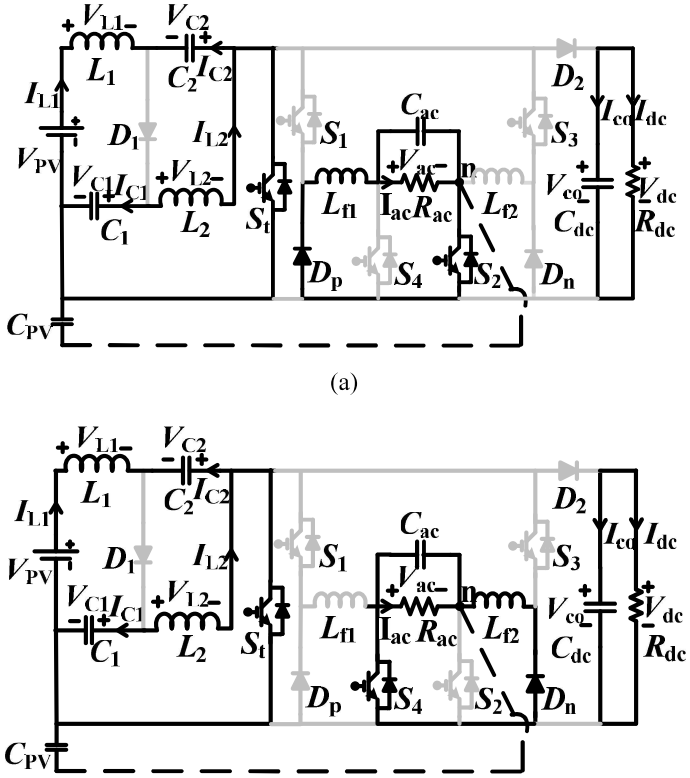

Fig. 3.3. Shoot through operating modes (a) Shoot-through state for V_{ac}>0. (b) Shoot-through state for V_{ac}<0.

When the S_t switch is ON, the inductors L_1 and L_2 start charging, drawing energy from the input source. At the same time, capacitors C_1 and C_2 begin discharging through the St switch, releasing the stored energy. During this period, diodes D_1 and D_2 remain in a reverse-biased state, preventing any current flow through them. Meanwhile, the output capacitor C_{dc} takes on the responsibility of supplying power to the load for the entire duration of this shoot-through state, ensuring a continuous and stable power supply.

In the AC section of the converter, the behaviour of the switches and diodes changes depending on the polarity of the AC voltage. When V_{ac} is positive ($V_{ac} > 0$), switch S_2 is turned ON. This allows the current through inductor L_{f1} to freewheel via switch S_2 and diode D_P, while diode D_N remains reverse-biased and blocks current flow, as illustrated in Fig. 3.3(a).

On the other hand, when V_{ac} is negative ($V_{ac} < 0$), switch S_4 is turned ON. In this scenario, the current flowing through inductor L_{f2} freewheels through switch S_4 and

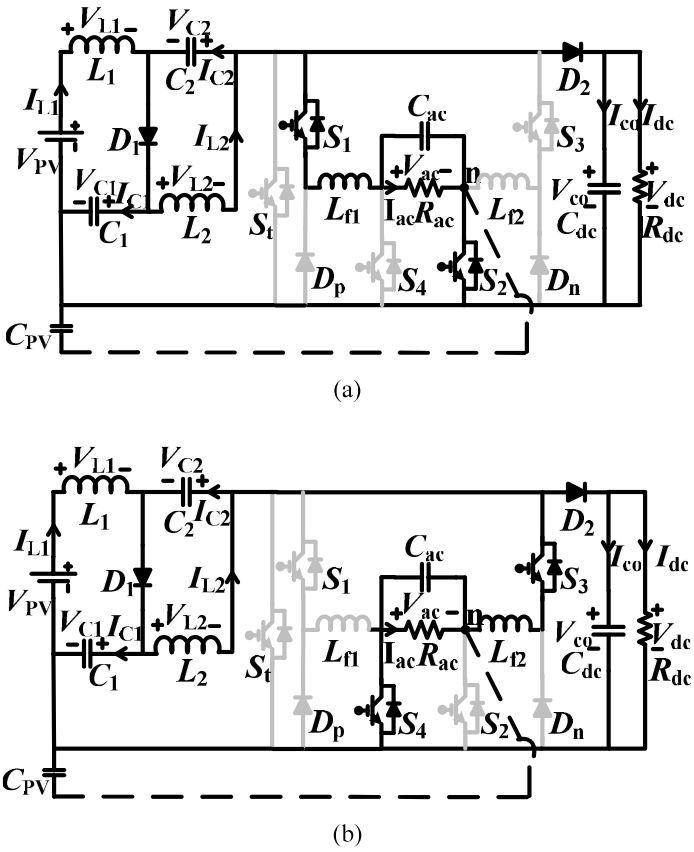

Fig. 3.4. Power state operating modes (a) Power state for V_{ac}>0. (b) Power state for V_{ac}<0.

diode D_N, while diode D_P becomes reverse-biased, as shown in Fig. 3.3(b). Overall, the shoot-through state is vital for maintaining the charging and discharging cycles of the passive components while keeping the load voltage stable and ensuring the proper operation of the AC section under varying input conditions.

➢ **Power state:** In the Power State of the L_2C_2-HC converter's operation, the switch S_t remains turned off, while the diodes D_1 and D_2 become forward biased, allowing current to flow through them. During this phase, the L_2C_2 network plays a crucial role in managing energy distribution. The capacitors C_1 and C_2 get charged by the inductors L_1 and L_2, and at the same time, they supply power to both the DC and AC loads. This happens seamlessly for both positive ($V_{ac} > 0$) and negative ($V_{ac} < 0$) cycles of the AC voltage.

Additionally, the capacitor C_{dc} also gets charged in this state while continuously supplying power to the DC loads, ensuring stable and efficient operation. When the AC voltage is positive ($V_{ac} > 0$), as illustrated in Fig. 3.4(a), switches S_1 and S_2 remain

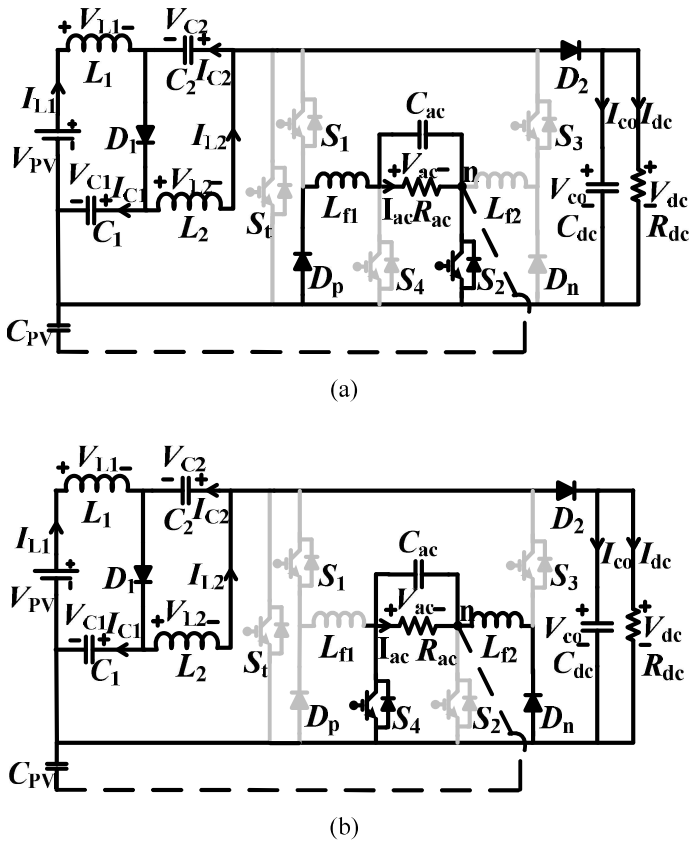

Fig. 3.5. Zero state operating modes (a) Zero state for V_{ac}>0. (b) Zero state for V_{ac}<0.

turned on, delivering power to the AC load R_{ac} through the AC filter components L_{f1} and C_{ac}. Similarly, when the AC voltage becomes negative ($V_{ac} < 0$), as shown in Fig. 3.4(b), switches S_3 and S4 take over, staying on and supplying the AC load R_{ac} with the same filter combination, L_{f1}, and C_{ac}.

- **Zero State:** In the Zero State of the L_2C_2-HC operation, the behaviour of the L_2C_2 network and the DC section remains the same as in the power state. However, the AC section behaves differently depending on the polarity of the AC voltage (V_{ac}). When $V_{ac} > 0$, as illustrated in Fig. 3.5(a), only switch S_2 remains ON, allowing the inductor current of L_{f1} to freewheel through S_2 and diode D_P. On the other hand, when $V_{ac} < 0$, as shown in Fig. 3.5(b), only switch S_4 stays ON, enabling the inductor current of L_{f2} to freewheel through S_4 and diode D_N. This selective switching helps manage current flow efficiently while maintaining the desired operational state.

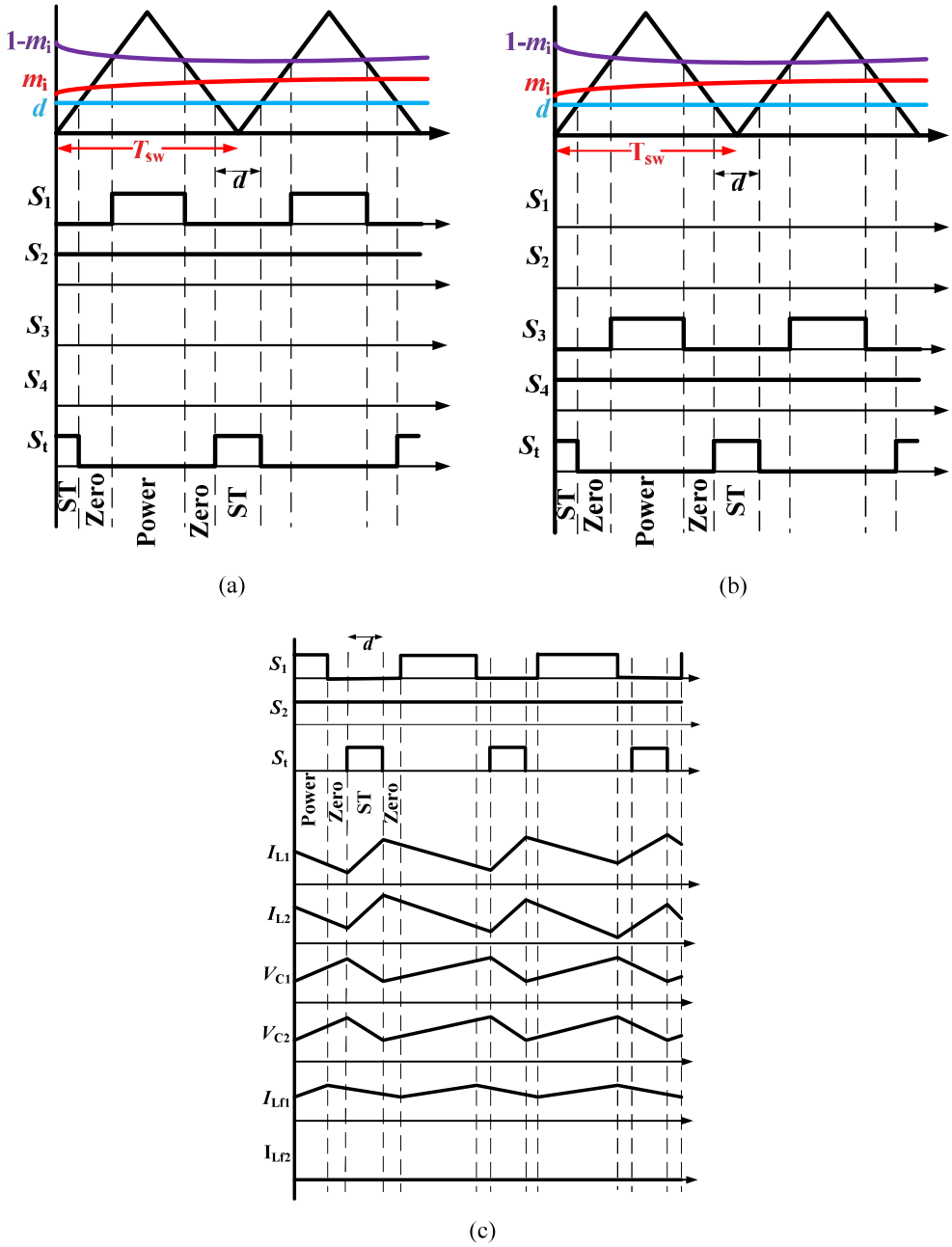

Fig. 3.6. Switching of MOHC (a) PWM switching waveform for $V_{ac} > 0$. (b) PWM switching waveform for $V_{ac} < 0$. (c) Waveform of the passive elements corresponds to switching pulses.

3.3.2. Switching of the proposed MOHC

A key factor in ensuring the desired performance of a converter is the effectiveness of its switching scheme i.e., Pulse Width Modulation (PWM) scheme. In this section, a novel PWM technique is specifically designed to control the operation of the L_2C_2-HC converter.

To generate the switching pulses for the switches S_t, S_1, S_2, S_3, and S_4, two signals are required: a sinusoidal wave with a peak value denoted by m_i, and a triangular wave operating at the switching frequency (f_s). The switching pulse for S_t is generated when the value of d is less than the instantaneous value of the triangular wave, regardless of whether the AC voltage (V_{ac}) is positive or negative.

When V_{ac} is positive ($V_{ac} > 0$), switches S_1 and S_2 are active. In this case, the value of 1 - m_i is compared with the triangular wave, and the switching pulse for S_1 is produced when 1 - m_i is less than the triangular wave. Simultaneously, switch S_2 remains in the ON state for the duration of the positive half-cycle, as illustrated in Fig. 3.6(a).

For the negative half-cycle of the AC voltage ($V_{ac} < 0$), switch S_4 remains ON. Here, the value of 1 - m_i is phase-shifted by 180° and compared with the triangular wave to determine the switching pulse, as depicted in Fig. 3.6(b). The resulting waveforms corresponding to the passive elements, aligned with the switching pulses, are presented in Fig. 3.6(c).

This novel PWM technique plays a crucial role in enhancing the efficiency and reliability of the L_2C_2-HC converter, offering improved control and reduced leakage current, which are essential for stable and efficient operation.

3.4. Design of the Proposed MOHC

The proposed Multi-Output Hybrid Converter (MOHC) has been carefully designed with a strong focus on efficient multi-output solutions. The design process of the L_2C_2-based Hybrid Converter (L_2C_2-HC) is thoughtfully divided into three key parts: the design of the L_2C_2 impedance network, the design of the DC filter, and the design of the AC filter. Each of these components plays a crucial role in ensuring the efficient and stable operation of the converter, and they are discussed in detail in the following sections.

3.4.1. Design of L_2C_2 Network

As mentioned earlier, the impedance network of the proposed converter, when (n = 2), consists of two inductors and two capacitors.

- **Design of C_1 and C_2**

The capacitors of the impedance network are designed on the basis of ripple factors considering the ripple factor of 1%, the C_1 and C_2 values of the converter can be designed using the equation:

$$I_{Cn} = C_n \frac{dV}{dt} \tag{3.1}$$

$$I_{Cn} = C_n \frac{dV}{d*T_s} = C_n \frac{dV*f_{sw}}{d} \tag{3.2}$$

Where d is the duty ratio, f_{sw} is the frequency, dV is the ripple voltage, and T_s is the switching time period.

- **Design of L_1 and L_2**

The inductors of the impedance network are designed on the basis of ripple factors considering the current ripple factor, the L_1 and L_2 values of the converter can be designed using the equation:

$$V_L = L\frac{dI}{dt} \tag{3.3}$$

$$V_L = L\frac{dI}{d*T_s} = L\frac{dI*f_{sw}}{d} \tag{3.4}$$

Where d is the duty ratio, f_{sw} is the frequency, dI is the ripple inductor current and T_s is the switching time period.

3.4.2. Design of filter DC capacitance (C_{dc})

Considering the case where all power is being transferred to the DC load i.e., 960W. thus the average output current at 230V output can be calculated as 4.2A

The average current flowing through the C_{dc} in shoot-through interval = 4.2A.

Considering the ripple factor of .1%, the C_{dc} value of the converter can be designed using the equation:

$$I_{Cn} = C_n \frac{dV}{dt} \tag{3.5}$$

$$I_{Cn} = C_n \frac{dV}{d*T_s} = C_n \frac{dV*f_{sw}}{d} \tag{3.6}$$

Where d is the duty ratio, f is the frequency, dV is the ripple voltage, and T_s is the switching time period.

Thus, the C_{dc} can be calculated as 438.26 µF.

The performance of the prototype was validated with the capacitance value 438.26 µF and above, and it was found that for C_{dc} = 470 µF, the performance of the experimental setup was best. Thus, the selected value of C_{dc} = 470 µF.

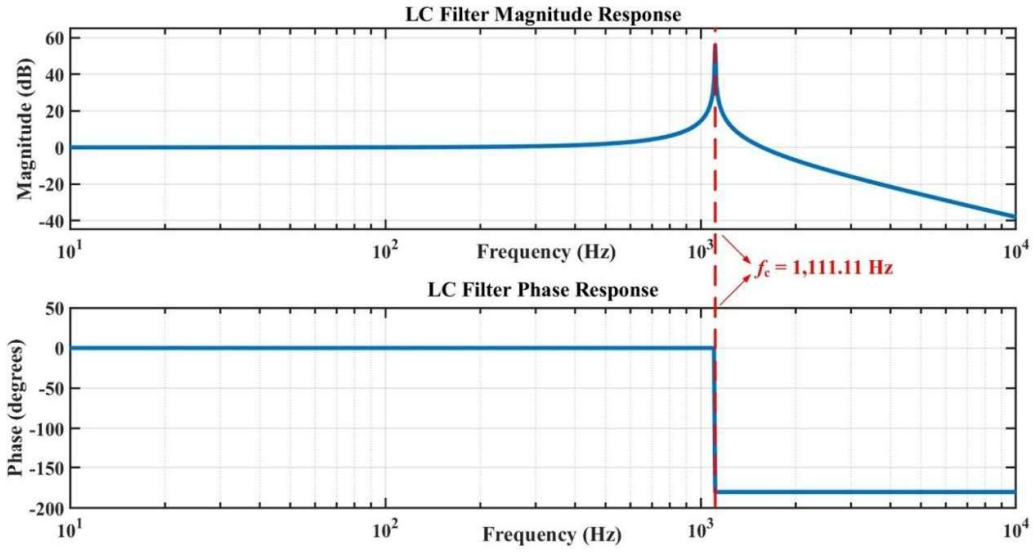

Fig. 3.7: Frequency response of LC filter.

3.4.3. Design of AC filters

LC filters have been widely used on the AC terminals of PWM inverters when the output voltages are the main control targets. The primary purpose of LC filters is to attenuate the voltage ripple that arises from inverter switching. This filter type is particularly well-suited for single-phase grid-connected inverters.

The passive components of the LC filter on the AC side (L_f and C_f) are designed by considering the corner frequency of L_f and C_f and the switching frequency (f_{sw}) of the controlled switches. The design of these AC side passive components involves selecting a corner/cut-off frequency equal to $f_s/9$, where f_s represents the switching frequency.

Choosing a cutoff frequency such as $f_s/9$ or approximately 1,111 Hz for a switching frequency of 10kHz provides a balance between filtering high-frequency harmonics and maintaining the integrity of the fundamental frequency. The choice and design of the LC filter can be further explained in 3 parts, i.e., 1) Filtering high-frequency harmonics, 2) How to maintain the integrity of fundamental frequency, and 3) Design of LC parameters.

- **Filtering High-Frequency Harmonics**

By choosing a cutoff frequency of around 1,111 Hz, i.e., $f_{sw}/9$, the LC filter is designed to significantly attenuate frequencies above this point. The LC filter will have a roll-off rate of 40 dB/decade beyond the cutoff frequency. This means that for every tenfold

increase in frequency beyond the cutoff frequency, the signal amplitude is reduced by 40 dB, as illustrated in Fig. 3.7.

At the switching frequency (10 kHz), which is about 9 times the cutoff frequency, the attenuation will be substantial, greatly reducing the presence of these high-frequency harmonics in the output.

- **Maintaining the Integrity of the Fundamental Frequency**

In AC power systems, the fundamental frequency (f_0) is typically 50 Hz or 60 Hz. For a 10 kHz switching frequency, the filter cutoff frequency ($f_{sw}/9$) is set at 1,111 Hz, significantly higher than the fundamental frequency. By establishing the cutoff frequency at 1,111 Hz, well above the fundamental frequency, the LC filter ensures that the fundamental component (50 Hz or 60 Hz) passes through with minimal attenuation. This is crucial for delivering a clean output at the fundamental frequency, which is essential for effective power delivery.

- **Design of the LC Parameter**

Keeping in view to eliminate the high-frequency harmonics and maintain the integrity of fundamental components, the passive components on the AC side can be selected to fulfill the equation (3.7).

$$\frac{f_s}{9} = \frac{1}{2\pi\sqrt{L_f C_f}} \tag{3.7}$$

Where f_{sw} is the switching frequency, L_f is the AC filter inductance, and C_f is the AC filter capacitance.

Additionally, the AC filter inductor is selected to limit the current ripple factor to no more than 20%. Therefore, the filter inductance can be determined using equation (3.8).

$$L_{f1} = L_{f2} = L_f = \frac{(V_{DC} - (V_{ac})_{PK})}{\Delta I_{Lf} * f_{sw}} * m_i \tag{3.8}$$

Where V_{DC} is the output DC voltage, $(V_{ac})_{PK}$ is the peak voltage of the AC grid, m_i is the modulation index, ΔI_{Lf} is the ripple current through the AC filter inductor, and f_{sw} is the switching frequency.

- **Specification of the hybrid converter**

The hybrid converter for a typical Indian home can be designed, featuring a 500 V maximum PV input, MPPT range of 100–490 V, and input current up to 26 A (Isc

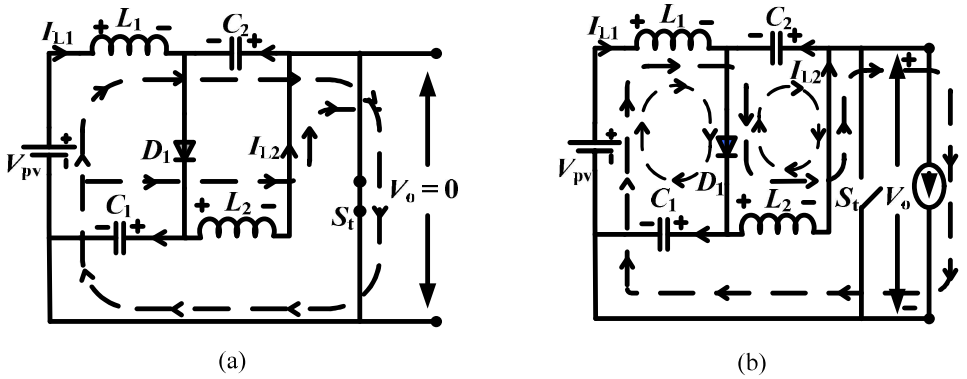

Fig. 3.8. L_2C_2 network analysis (a) dTs mode. (b) (1-d)Ts mode.

31.2 A). It provides 110 V AC at 50 Hz (44 A max) and 240 V DC (21 A max), with a total output capacity of 5000 W, suitable for combined AC/DC household loads.

3.5. Steady State analysis

For the steady-state analysis of the hybrid converter, the performance of both the DC and AC output sections is largely influenced by the behaviour of the L_2C_2 impedance network. This network operates in two distinct modes: the shoot-through state and the non-shoot-through state.

In the shoot-through state, which lasts for a duration of (dT_s) where d is the shoot-through duty cycle and T_s is the total switching period, both the upper and lower switches of a phase leg are simultaneously turned on, creating a short circuit across the inverter's input. This mode is illustrated in Fig. 3.7(a) and plays a crucial role in boosting the voltage and stabilizing the system.

The non-shoot-through state occurs during the remaining (1-d)T_s interval. This state is further divided into two phases: the zero state, where no power is delivered, and the power state, where energy flows from the input source to the load. This operation is depicted in Fig. 3.7(b).

The mathematical equations that describe and govern the behaviour of the L_2C_2 network in both states are provided below, forming the foundation for the steady-state analysis of the converter's performance.

a) Shoot-through State: (3.9)

$$\left.\begin{aligned} V_{L1} &= V_{PV} + V_{C2} \\ V_{L2} &= V_{C1}; \\ I_{C1} &= -I_{L2} \\ I_{C2} &= -I_{L1} \\ V_0 &= 0 \end{aligned}\right\}$$

b) Non-shoot through State:

$$\left.\begin{aligned} V_{L1} &= V_{PV} - V_{C1} \\ V_{L2} &= -V_{C2} \\ I_{C1} &= I_{D1} - I_{L2} \\ I_{C2} &= I_{D1} - I_{L1} \\ V_0 &= V_{C1} + V_{C2} \end{aligned}\right\} \tag{3.10}$$

By applying the volt-sec balance across the capacitors in Shoot through and non-shoot through state. The L_2C_2 network the voltage across the capacitors can be calculated as:

$$V_{C1} = \left(\frac{1-d}{1-2d}\right) V_{pv} \tag{3.11}$$

$$V_{C2} = \left(\frac{d}{1-2d}\right) V_{pv} \tag{3.12}$$

From (3.9), (3.10), (3.11), and (3.12), the peak voltage across the V_o for L_2C_2 network can be calculated as:

$$\widehat{V_o} = V_{C1} + V_{C2} = \left(\frac{1}{1-2d}\right) V_{pv} \tag{3.13}$$

Similarly, the V_o corresponding for expandable L_nC_{2n-2} can be calculated as:

$$V_{C1} = \left(\frac{1-(n-1)d}{1-nd}\right) V_{pv} \tag{3.14}$$

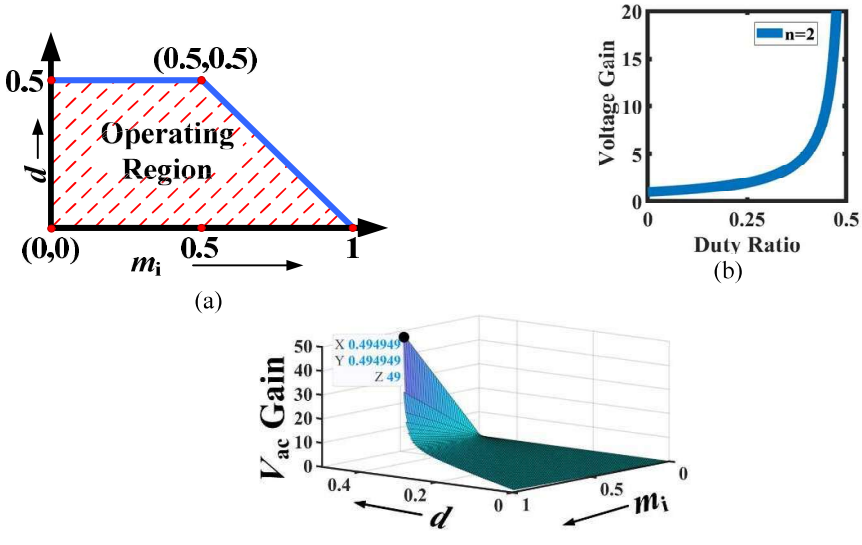

Fig. 3.9. Operating characteristics of proposed MOHC (a) The operating range for d and m_i; (b) DC gain Characteristics; (c) AC voltage gain characteristics with reference to d and m_i.

$$V_{C2} = V_{C3} = V_{C4} = \ldots\ldots = V_{Cn} = \left(\frac{d}{1-nd}\right) V_{pv} \tag{3.15}$$

$$\widehat{V_o} = V_{C1} + V_{C2} + \ldots\ldots\ldots + V_{Cn} = \left(\frac{1}{1-nd}\right) V_{pv} \tag{3.16}$$

Thus, by the inclusion of a capacitive filter (C_{dc}) in the DC side the DC voltage (V_{dc}) can be calculated as:

$$V_{dc} = \left(\frac{1}{1-2d}\right) V_{pv} \tag{3.17}$$

The output voltage corresponding to AC section of the L_2C_2-HC is a function of both d and m_i thus the AC output can be calculated as:

$$(V_{ac})_{pk} = \left(\frac{m_i}{1-2d}\right) V_{pv} \tag{3.18}$$

Similarly, the output voltage corresponding to expandable L_nC_{2n-2}-HC can be expressed as:

$$V_{dc} = \left(\frac{1}{1-nd}\right) V_{pv} \tag{3.19}$$

$$(V_{ac})_{pk} = \left(\frac{m_i}{1-nd}\right) V_{pv} \tag{3.20}$$

Since the same set of switches controls the hybrid converter, therefore, there is a compromise between d and mi, i.e., $d+m_i \leq 1$. Whereas in L_2C_2-HC, the range for mi is 0 to 1. On the other hand, the operating range for d is 0 to 0.5. Thus, the operating region for mi can be made wider, i.e., $m_i \geq 0.5$, for a better quality of AC output; the operating regions of d and m_i can be shown in Fig. 3.9(a). DC Voltage gain corresponding to d is shown in Fig. 3.9(b), and AC voltage gain with reference to d and m_i is shown in Fig. 3.9(c).

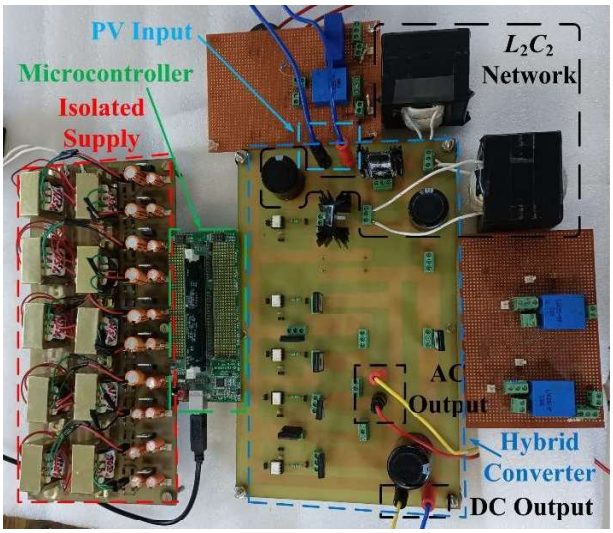

Fig. 3.10: Photograph of experimental setup.

TABLE 3.1 HARDWARE SPECIFICATION OF MOHC	
Switch	IKW75N60H3
Diode (D_1, D_2, D_P and D_n)	RURG8060
Inductors (L_1 and L_2)	1.256 mH
Capacitors (C_1 and C_2)	180 uF
DC Filter Capacitance (C_{dc})	470 uF
AC Filter Inductance (L_{f1} and L_{f2})	3 mH
AC Filter Capacitance (C_{ac})	10 uF
Parasitic Capacitance (C_{PV})	110 uF
DC Load Resistance (R_{dc})	88 ohm
AC Load Resistance (R_{ac})	55 ohm

3.6. Experimental Verification

To demonstrate and validate the practical feasibility of the proposed concept, a laboratory prototype with a power rating of 960 W has been developed.

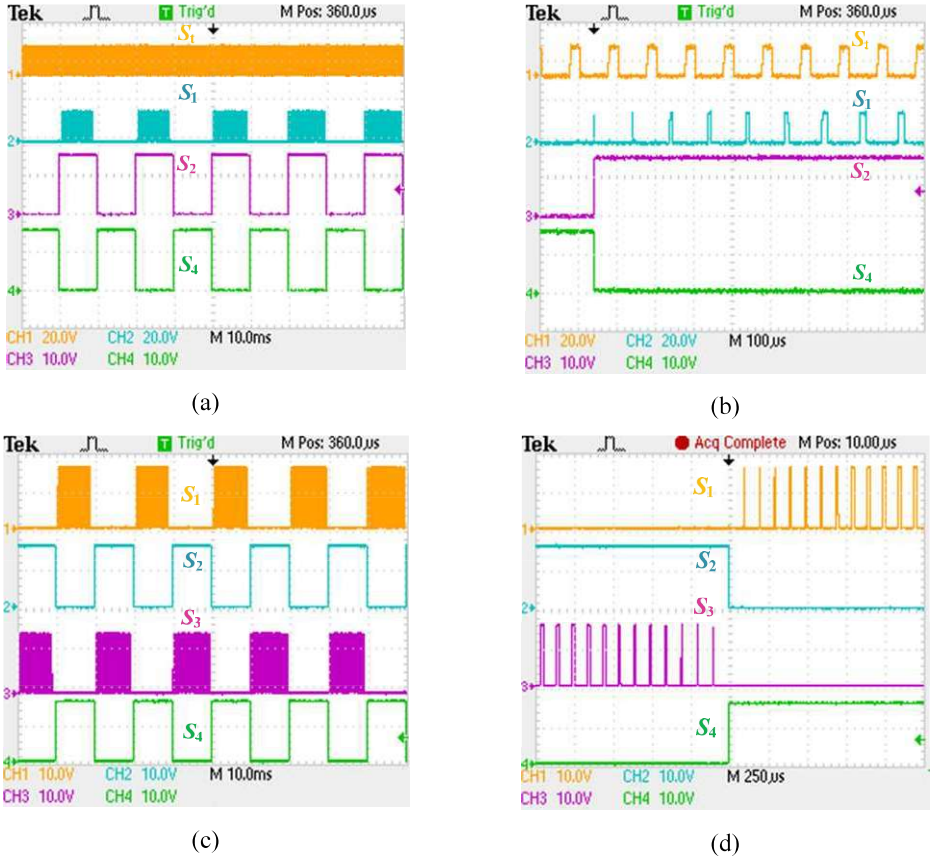

Fig. 3.11. Switching waveform (a) Switching waveform of S_t, S_1, S_2, S_4. (b) Zoomed view of switching waveform of S_t, S_1, S_2, S_4. (c) Switching waveform of S_1, S_2, S_3, S_4. (d) Zoomed view of switching waveform of S_1, S_2, S_3, S_4.

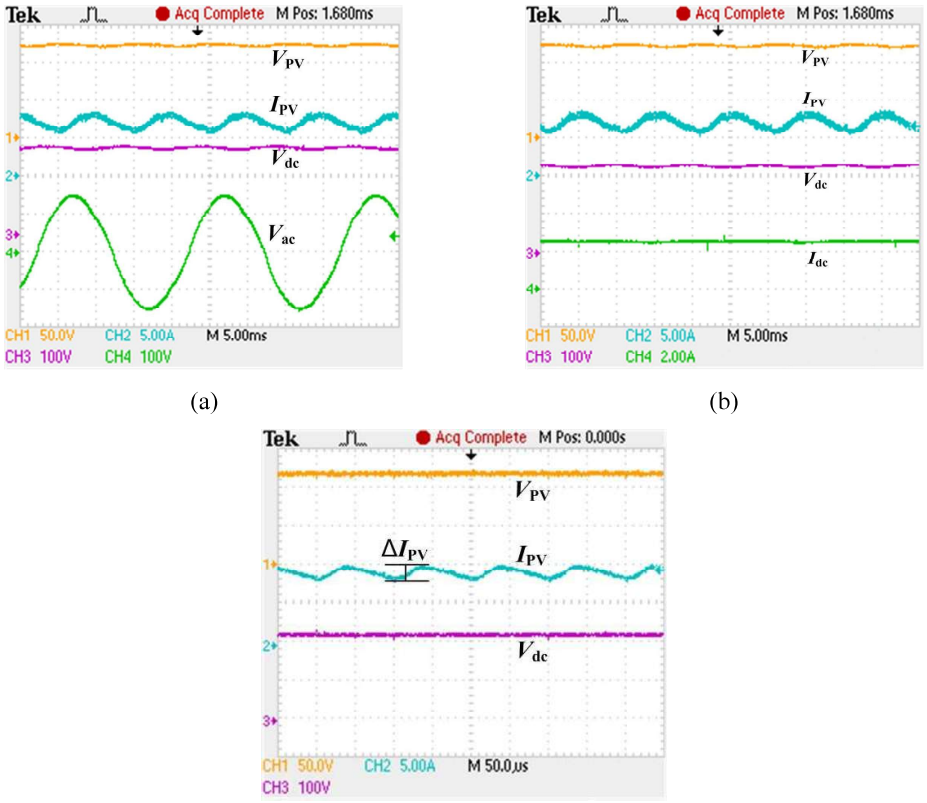

Fig. 3.12 Multi-Output characteristics of proposed MOHC (a) Input voltage and current (V_{PV} and I_{PV}), DC and AC output voltage (V_{dc} and V_{ac}). (b) DC output voltage and current (V_{dc} and I_{dc}). (c) Ripple value of Input PV current and output DC voltage.

This prototype is designed to operate in both standalone mode and grid-connected mode, showcasing the versatility of the L_2C_2-based Hybrid Converter (L_2C_2-HC).

The design parameters of the L_2C_2-HC have been carefully selected based on component availability and system requirements, ensuring optimal performance and ease of implementation. These design specifications are summarized in Table 3.1. Additionally, a photograph of the assembled prototype, illustrating the physical realization of the proposed topology, is presented in Fig. 3.10.

3.6.1. Switching Waveform

The switching waveform of the proposed converter is shown in the Fig. 3.11. In Fig. 3.11(a), the PWM waveform showcases the switching actions of switches S_t, S_1, S_2, and S_4, with a closer examination presented in Fig. 3.11(b). Additionally, Fig. 3.11(c) exhibits the switching waveform for switches S_t, S_1, S_2, and S_4, while an enlarged view is depicted in Fig. 3.11(d).

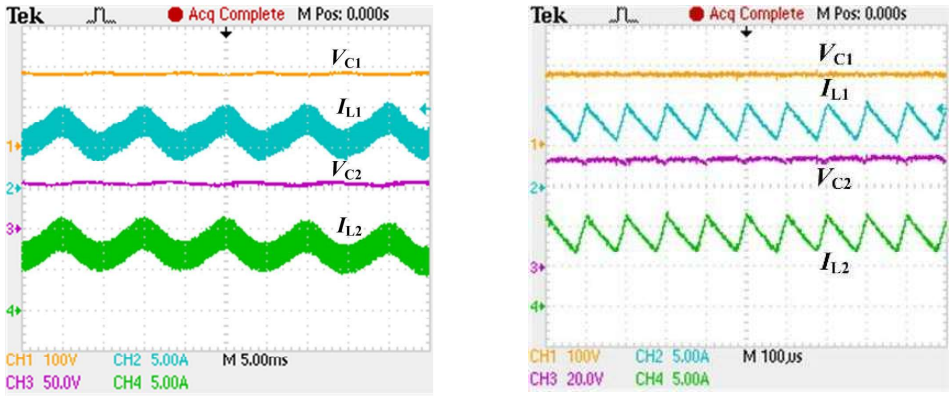

(a) **(b)**

Fig. 3.13. L_2C_2 Characteristics (a) Voltages and currents of the L_2C_2 network. (b) zoomed view of voltages and currents of the L_2C_2 network.

3.6.2. Multi-Output Characteristics of the Proposed MOHC

Fig. 3.13(a) showcases the attainment of a simultaneous DC output voltage (V_{dc}) of 230V, along with an AC output voltage of 110V rms, with an input voltage (V_{PV}) of 120V and an input current of 8A. In Fig. 3.13(b), the DC voltage of 230V is depicted alongside a DC current of 2.6A, thus affirming the multi-output characteristics of the proposed L_2C_2-HC. As shown in Fig. 3.13(c) the peak-to-peak current value of the inductors, ΔI_{PV}, is 1.6 A, and the Ipv current is 8 A. This results in a ripple factor of 20% at full rating and to ensure smooth operation on the DC side, the DC output voltage has been designed to be ripple-free.

3.6.3. L_2C_2 Characteristics of the proposed L_2C_2-HC

Fig. 3.12 provides a detailed illustration of the voltage and current waveforms associated with the L_2C_2 network. In this network, the inductor currents are measured as $I_{L1} = I_{L2} = 8$A, while the capacitor voltages are observed at $V_{C1} = 180$V and $V_{C2} = 55$V. A notable characteristic of this network is the presence of a double-frequency harmonic component. This harmonic, occurring at twice the switching frequency ($2 * f_s = 2 * 50 = 100$ Hz), arises due to the inverting operation of the Multi-Output Hybrid Converter (MOHC). This behaviour is a key feature of the L_2C_2 network's dynamic response.

For a clearer understanding of the waveform characteristics, Fig. 3.12(b) offers a zoomed-in view of the portion shown in Fig. 3.12(a), enabling a closer inspection of the voltage and current variations and the impact of the harmonic component.

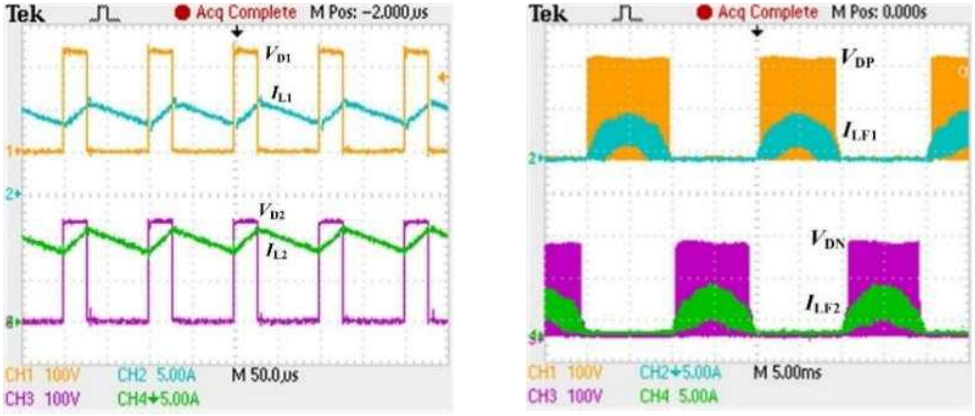

(a) (b)

Fig. 3.14. Voltage and current stress across diodes (a) Voltage stress across D_1 and D_2 along with inductor current. (b) Filter inductor currents (I_{L1} and I_{L2}) and diodes voltages stress (V_{DP} and V_{DN}).

3.6.4. Voltage and Current Stress Across Diodes

Fig. 3.14(a) illustrates the voltage stress experienced by the diodes D_1 and D_2 of the L_2C_2 network, along with the corresponding inductor currents I_{L1} and I_{L2}. This representation provides valuable insight into the electrical behaviour and performance of these circuit components.

Meanwhile, Fig. 3.14(b) highlights the voltage stress across the diodes in the AC section, specifically D_P and D_N, accompanied by the current waveforms of the filter inductors, I_{Lf1} and I_{Lf2}. This detailed view helps to better understand the interaction between voltage and current in the filtering stage, emphasizing the importance of these elements in maintaining system stability and power quality.

3.7. Summary

In this chapter, the development of the proposed L_nC_{2n-2} network-based multi-output converter has been thoroughly explained for an arbitrary number of stages, 'n'. To validate the concept and its practical feasibility, the case of '$n = 2$' has been specifically chosen — resulting in the L_2C_2 network-based Multi-Output Hybrid Converter (MOHC). The operating principles and different modes of this converter have been carefully discussed, along with the Pulse Width Modulation (PWM) scheme used for its switching operation.

A crucial aspect of any power converter is the proper design of its components. Therefore, the design considerations of the L_2C_2 impedance network, DC filter, and AC filter have been presented in detail. These elements play a key role in ensuring the converter's efficient and stable performance.

To validate the theoretical analysis and design, a 960 W experimental prototype of the proposed converter has been developed and tested. The results from this prototype confirm the converter's practical performance and its potential for real-world applications.

However, this chapter does not address certain important aspects of the converter's performance. Specifically, the leakage current analysis, technical advantages, and performance benefits of the proposed topology, as well as the efficiency performance and loss distribution, remain unexplored here. These critical aspects will be discussed in depth in the next chapter.